

## Enhanced Collimated GeV Monoenergetic Ion Acceleration from a Shaped Foil Target Irradiated by a Circularly Polarized Laser Pulse

M. Chen, A. Pukhov, and T. P. Yu

*Institut für Theoretische Physik I, Heinrich-Heine-Universität Düsseldorf, Düsseldorf 40225, Germany*

Z. M. Sheng

*Department of Physics, Shanghai Jiao Tong University, Shanghai 200240, China  
and Beijing National Laboratory of Condensed Matter Physics, Institute of Physics, Beijing 100080, China  
(Received 17 March 2009; published 10 July 2009)*

Using multidimensional particle-in-cell simulations we study ion acceleration from a foil irradiated by a circularly polarized laser pulse at  $10^{22}$  W/cm<sup>2</sup> intensity. When the foil is shaped initially in the transverse direction to match the laser intensity profile, three different regions (acceleration, transparency, and deformation region) are observed. In the acceleration region, the foil can be uniformly accelerated for a longer time compared to a usual flat target. Undesirable plasma heating is effectively suppressed. The final energy spectrum of the accelerated ion beam in the acceleration region is improved dramatically. Collimated GeV quasi-monoenergetic ion beams carrying as much as 19% of the laser energy are observed in multidimensional simulations.

DOI: 10.1103/PhysRevLett.103.024801

PACS numbers: 41.75.Jv, 52.38.Kd

Ion acceleration by ultraintense ultrashort laser pulse interacting with solid targets has been extensively studied in the last decade [1] due to a number of prospective applications, such as proton therapy [2], proton imaging [3], ion beams ignition for laser fusion [4], etc. Recently along with the progress of plasma mirror technology, the ion acceleration from laser-foil interaction has attracted much more attention. It has been shown in one-dimensional (1D) particle-in-cell (PIC) simulations that by use of circularly polarized (CP) laser pulses monoenergetic ion beams can be especially generated in principle [5,6]. The key effect here is the suppression of electron heating [6,7] because of the absence of the oscillating part in the ponderomotive force for a CP pulse, which otherwise would disperse the plasma electrons in space and destroy the monoenergetic acceleration. Theoretical models and simulations based on 1D geometry have shown a very promising scaling law for the final energy spectrum of the accelerated ions. It predicts quasi-monoenergetic GeV ion beams for sufficiently long driver laser pulses [5]. This kind of acceleration belongs to the laser pressure dominated acceleration (LPDA).

However, multidimensional simulations show that the acceleration structure is not so stable [8,9]. Electrons and ions are inevitably dispersed transversely when the target is deformed and heated by the driving pulse. Besides these, instabilities are also another fatal problem. The transverse instability of the accelerating structure limits the maximum energy of the accelerated ions and broadens the final energy spectrum. To overcome this, the laser mode effects have recently been considered [9]. In this Letter we restudy the problem by considering the target shaping, which might be easier to realize in experiments. The target fab-

rication has already been applied before for the ion acceleration in the target normal sheath acceleration regime, where the optimization of ion energy spectrum can be achieved by target shaping [10]. In the LPDA regime, the target has usually a thickness of a few hundred nanometers. Fortunately, due to the rapid progress in the nanotechnology, structured nano thickness targets can be engineered today. In the present study, by use of 2D and 3D parallelized PIC code (VLPL) [11] we show how to optimize the collimation and monochromaticity of the accelerated ion beams via the target shaping. By optimal matching, a collimated, GeV quasi-monoenergetic proton beam can be generated by a CP laser pulse at  $10^{22}$  W/cm<sup>2</sup> intensity incident on a shaped foil target (SFT) with the thickness of a few hundreds nanometer.

First we study the target deformation under the interaction of a laser pulse. From the momentum conservation law between the laser pulse and the target, the evolution of the target velocity ( $\beta$ ) can be described as:

$$\frac{d\beta}{dt} = \frac{1}{2\pi n_0 m_i c} \frac{E^2(t, x, r)}{l_0} \frac{1}{\gamma^3} \frac{1 - \beta}{1 + \beta}, \quad (1)$$

where  $E$  indicates the laser electric field,  $n_0$  and  $l_0$  are the target initial density and thickness, respectively. It shows that the energy spread of accelerated ions depends on the transverse variation of the local ratio of laser intensity to the target area density. The distance the ions pass in the target is:  $s(r) \propto E^2(t, x, r) l_0^{-1}$ . An initially flat target is inevitably deformed, if the laser intensity is not uniform transversely. The target deformation quickly destroys the acceleration structure and deteriorates the beam quality. From Eq. (1) we see that a target can be kept flat if its areal density  $\sigma = n_0 l_0$  is shaped properly. For the usual trans-

versely Gaussian pulse, one can use a target with the Gaussian thickness distribution as shown in Fig. 1(a). In the following simulations, the distribution of the target thickness is:

$$l = \max\{l_1, l_0 \times \exp[(-r^2/\sigma_T^2)^m]\}. \quad (2)$$

Here  $r$  is the transverse distance to the laser axis,  $l_1$ ,  $l_0$ ,  $\sigma_T$ ,  $m$  are the shape parameters, which are shown in Fig. 1(a).

We begin with 2D simulations to find the optimal parameter region because they are computationally less expensive than simulations in the full 3D geometry. The total simulation box is  $32\lambda(x) \times 32\lambda(y)$  with  $\lambda$  representing the laser wavelength, which corresponds to a grid of  $3200(x) \times 320(y)$ . The time step of the simulation is  $0.008T_0$ , here  $T_0 = 3.33$  fs is the laser period. The foil plasma consists of two species: electrons and protons. They are initially located in the region  $5\lambda \leq x \leq 5.3\lambda$  with the density of  $n = 100n_c$ , where  $n_c = \omega^2 m_e / 4\pi e^2$  is the critical density for the laser pulse with the frequency  $\omega$ . For 1  $\mu\text{m}$  laser pulse it is  $n_c = 1.1 \times 10^{21}/\text{cm}^3$ . We use 216 particles in every simulation cell. Here, we present the results for a shaped foil target whose parameters are  $l_0 = 0.3\lambda$ ,  $\sigma_T = 7\lambda$ ,  $l_1 = 0.15\lambda$ ,  $m = 1$ . For the flat target, we just set  $l_1 = 0.3\lambda$ , other parameters are the same. Thus, the total number of ions in the center part of the SFT is originally less than that in the case of the flat target. The target is shaped along the  $Y$  direction in the 2D case and in the radial direction in the 3D case. The normalized amplitude of the laser electric field at the focus is  $a = a_0 \exp(-r^2/\sigma_L^2)$  with  $a_0 = eE_0/m\omega c = 100$  and  $\sigma_L =$

$8\lambda$ . This corresponds to the laser intensity of  $I = 2.76 \times 10^{22}$  W/cm<sup>2</sup> for the assumed wavelength  $\lambda = 1$   $\mu\text{m}$ . The laser pulse has a trapezoidal temporal intensity profile (linear growth—plateau—linear decrease), with  $1\lambda/c - 8\lambda/c - 1\lambda/c$ . Thus, the total laser pulse energy is about 793.5 J. At  $t = 0$  the laser pulse enters the simulation box from the left boundary.

Figure 1(b) shows the energy spectrum of the accelerated ions at  $t = 30T_0$  and  $t = 40T_0$  for the flat and shaped targets in the 2D-PIC simulations. In the simulation, both the particles and fields satisfy periodical boundary conditions in the transverse direction ( $Y, Z$ ) and they are within a region of 0.1  $\mu\text{m}$  long in the  $Z$  direction. So the number of the particles is smaller than the real value in 3D conditions. The flat target produces no obvious peak structure in the spectrum. Instead, the spectrum shows an exponential decrease like  $dN/dE_k \propto \exp(-E_k/E_{\text{eff}})$  with  $E_{\text{eff}} \approx 500$  MeV for  $E_k > 300$  MeV and a cutoff energy 1.7 GeV at  $40T_0$ .

When a SFT is used with the transverse shape factor  $\sigma_T = 7\lambda$ , the spectrum becomes quasi-monoenergetic. The energy of the peak is about 1.2 GeV at  $t = 40T_0$ , which is very close to the analytical values obtained by solving Eq. (1). As we can see the maximum ion energy at  $t_{\text{sim}} = 40T_0$  in 2D simulation is a bit higher than the 1D theoretical value. This is because of reduction of the target area density during the interaction. Although the maximum cutoff energy of the ions in the SFT case is lower than that in the flat target case, much more protons are accelerated in a much narrower region, which benefits the further application of the accelerated proton beams.

To show the polarization effect, a linearly polarized laser pulse is used. The magenta dashed line in Fig. 1(b) shows the ion energy spectrum at  $t = 40T_0$ . In this case, the electrons are easily heated and scattered by the oscillating part of the laser ponderomotive force. The target becomes transparent to the pulse very soon. Ions are only accelerated by the spatially dispersed electron cloud and cannot get as high energy as in the CP pulse case. The spectrum is again exponential with a lower cutoff.

Figures 2(a) and 2(b) show the spatial distribution of ions at  $t = 25T_0$  in the two simulations. The target shaping leads to a more transversely uniform ion acceleration. The initially flat target, in contrary, is deformed and a natural cone builds up during the interaction. The laser intensity distribution shown in Figs. 2(c) and 2(d) confirms this. The natural cone focuses the lateral laser energy to the center and thus reinforces the on-axis ion acceleration. On one hand, this effects destroys the foil, but on the other hand it leads to the higher cutoff energy as shown in Fig. 1(b). This is similar with the pre-cone-target used by Cao *et al.* [12]. However, in the present case the cone makes the chromaticity of the accelerated ions worse. When the laser pulse irradiates the cone, electrons are easily extracted out by the laser field from the inner wall of the cone and heated because of the oblique incidence. These heated electrons disperse in space and pollute the acceleration structure,

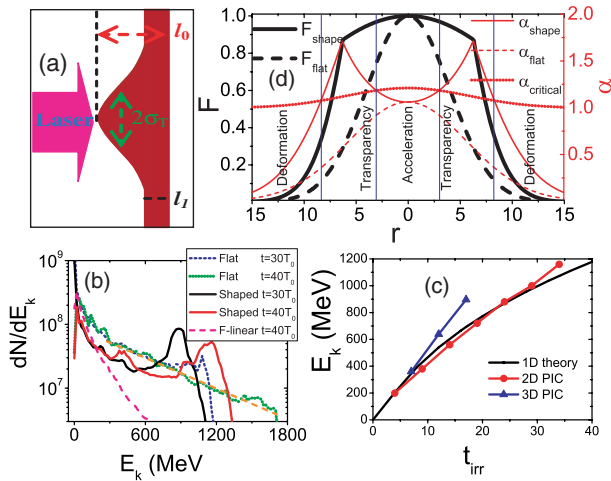


FIG. 1 (color online). (a) Layout of shaped target. (b) Energy spectrum of ions. The orange (light gray) dashed line shows the exponential decrease of the spectrum. (c) Energy evolution of accelerated ions from multidimensional PIC simulations and 1D theoretical calculation. Here  $t_{\text{irr}}$  represents the time of laser irradiation on target. (d) Distribution of the acceleration factor (thick lines) and transparency factor (thin lines) of the target. Solid and dashed lines correspond to shaped target case ( $l_0 = 3\lambda$ ,  $l_1 = 1\lambda$ ) and flat target case ( $l_0 = l_1 = 3\lambda$ ), respectively. Here  $\sigma_L = 8\lambda$ ,  $\sigma_T = 6\lambda$ .

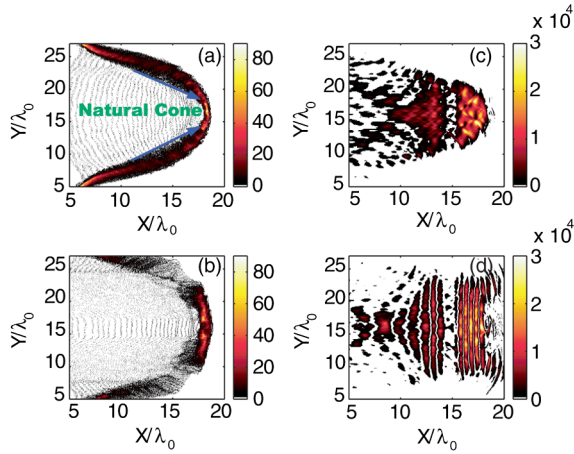


FIG. 2 (color online). Spatial density distribution of ions in the flat target case (a) and in the SFT case (b) at  $t = 25T_0$ . Spatial distribution of the laser intensity ( $E_y^2 + E_z^2$ ) in the flat target case (c) and in the SFT case (d) at  $t = 25T_0$ .

which destroys the monoenergetic character of the ion spectrum. A shaped target can reduce these undesirable effects dramatically.

The angular distributions of the accelerated ions in the two target cases are presented in Fig. 3. It shows that in the SFT case the accelerated ions mainly move forward. However, in the flat target case, only a small portion of the highly energetic ions moves forward. Ions in the middle energy range get a considerable transverse momentum. From the simulation, we find the average emission angle for the ions whose energy is larger than 1 GeV is about  $2.7^\circ$  in the SFT case and  $5.22^\circ$  in the flat target case. The number of ions in this energy range is 1.9 times larger in the SFT case as compared with the flat target. Clearly, both the collimation and the total flux of accelerated ions are improved in the SFT case.

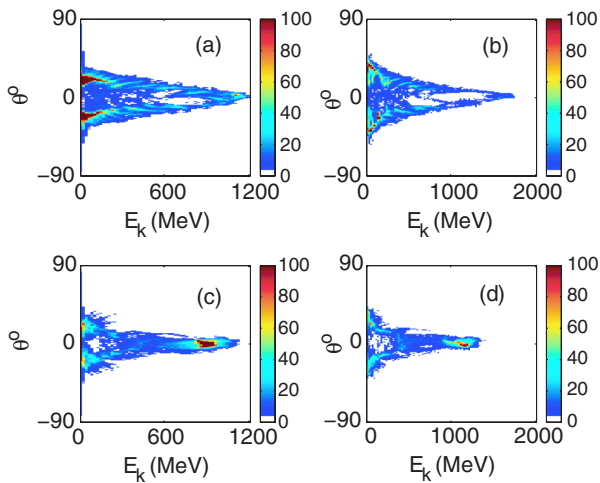


FIG. 3 (color online). Angular distribution of ions at  $t = 30T_0$  and  $t = 40T_0$ . (a) and (b) correspond to flat target case; (c) and (d) correspond to SFT case. The color represents the relative ion number.

To ensure that these effects are not a 2D artefact, we perform full 3D simulations. For the shaped target, we use  $\sigma_T = 6\lambda$  in the 3D simulation. The initial position of the target is moved to  $x = 2\lambda$  to reduce the computational cost. The laser longitudinal profile is also reduced to be:  $1\lambda/c - 5\lambda/c - 1\lambda/c$ . Other parameters are the same as those in the 2D simulation above. The electron and ion distributions at  $t = 20T_0$  are shown in Fig. 4. As we see, in the SFT case a stable compact target sheath with thickness of about  $0.7\lambda$  breaks out from the rest of the foil and is accelerated by the laser pulse. In contrast, in the flat target case, Fig. 4(c) displays a continuously dispersing ion density distribution. The ion energy spectrum shown in Fig. 4(d) also confirms the quasi-monoenergetic peak in the SFT case. The number of ions with energy larger than 800 MeV are  $5.09 \times 10^{11}$  and  $6.63 \times 10^{11}$  for the flat target and shaped target, respectively. And their total energies are  $5.05 \times 10^{14}$  MeV and  $6.16 \times 10^{14}$  MeV, the conversion efficiencies are 15.57% and 19%, respectively. It deserves to note that in the 3D case the ion energies are higher than the 1D analytical prediction as shown in Fig. 1(c). The calculated peak value of the ion energy is 635 MeV at  $t_{\text{sim}} = 20T_0$ ; however, the simulation result is 910 MeV. This difference is also due to the target dispersion. In the 3D geometry electrons disperse easily in the transverse direction, then the laser pulse can also transmit through the lateral parts of the target much easier. Central electrons are dragged out by the transmitted pulse and further disperse in space, which decreases the effective central target area density. Consequently part of the ions in the center part receive a stronger acceleration. Generally we find the 1D estimation gives a higher energy conversion efficiency and a lower peak energy.

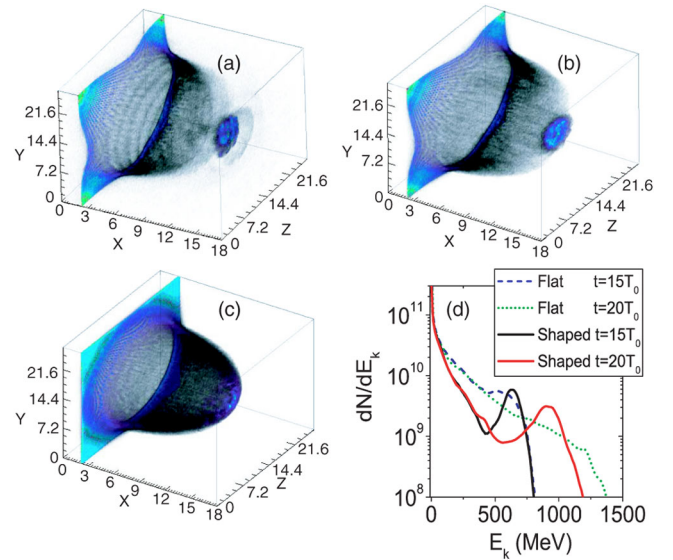


FIG. 4 (color online). Spatial density distribution of electrons (a) and ions (b) in the 3D simulation at  $t = 20T_0$ . (c) Spatial density distribution of ions in the flat target case. (d) Energy spectrum of ions in the SFT case and flat target case. At  $t = 20T_0$  the laser pulse has left away from the target.

To explain the effects of the target shape clearly we show the transverse distribution of the acceleration factor ( $F = a^2/l$ ) and the transparency factor ( $\alpha = a/\pi nl$ ) of the target in Fig. 1(d).  $F$  is normalized by the maximum value in the target center, which directly relates to the target deformation. As we see when a shaped target is used, the acceleration factor  $F$  is almost uniform in the matched region. However, once  $F$  is uniform the transparent factor ( $\propto a/nl$ ) varies. The latter describes the ratio of the forces due to the laser pressure  $F_P$  and the charge separation between ions and electrons  $F_E$ :

$$F_P = \frac{mc^2\lambda}{e^2} a^2 \frac{1 - \beta_e}{1 + \beta_e} dS, \quad F_E = \frac{mc^2\lambda}{e^2} \pi^2 n^2 l^2 dS. \quad (3)$$

Here the force  $F$  and the area element  $dS$  are normalized by  $m\omega c$  and  $\lambda^2$ , respectively;  $\beta_e$  is the normalized velocity of the compressed electron layer. When  $F_P > F_E$ , electrons are completely pushed out of the target and the target becomes transparent to the laser pulse later. It corresponds to the transparency factor  $\alpha$  larger than the critical value  $\alpha_c = \sqrt{(1 + \beta_e)/(1 - \beta_e)}$ . Considering a finite ion mass and relativistic effects, we take  $\beta_e = \beta_h = a/(a + \sqrt{mn})$ , where  $\beta_h$  is the relativistic hole boring velocity [13]. The ion motion in the pre-hole-boring process is usually omitted; however, it is critical to get the correct value for the transparent thickness of the target. As shown in Fig. 1(d), when a shaped target is used it evolves into three different regions. In the center, an acceleration region exists, where it is opaque to the laser pulse and the acceleration is uniform. Nearby is a transparency region and the laser pulse transmits through it. The outside part is the deformation one, where both acceleration and deformation happen. All these three parts can be observed in Figs. 2(b), 4(a), and 4(b). However, for a flat target, the transparent factor is always lower than the critical value and the velocity is not uniform, all the target is in the deformation region.

By considering the space of the transparency region, we can get the maximum final radius of the accelerated ion bunch:  $r_b \approx \sigma_T \sigma_L \sqrt{\ln(\alpha_c/\alpha_0)/(\sigma_L^2 - \sigma_T^2)}$ , here  $\alpha_0 = a_0/\pi n_0 l_0$ . So the best choice of  $l_1$  and  $\sigma_T$  should be:  $l_1 \leq l_0 \exp(-r_b^2/\sigma_T^2)$  and  $\sigma_T < \sigma_L$ . This corresponds to  $r_b = 3.1$ ,  $l_1 \leq 0.23$  if we take  $\sigma_T = 6$  and  $\alpha_c = 1.19$  from Fig. 1(d). The bunch size is close to our 3D simulation ( $r_b \approx 3.5$ ). In simulations, we also check the sensitivity of the results on the parameters  $l_1$  and  $\sigma_T$ . If we vary  $l_1$  only, but keep  $l_1 < 0.2$ , the monoenergetic part of the final spectrum almost does not change, only the lower energy part increases with  $l_1$ . This means that only the ions in the center part of the target contribute to the final monoenergetic peak. Correspondingly, the target width  $\sigma_T$  is a critical parameter for the final spectrum. We find in the 2D geometry that when  $\sigma_T/\sigma_L \approx 0.85$ , the optimum spec-

trum appears. For the present simulation, when  $\sigma_T/\sigma_L \in [0.4, 1.0]$  the monoenergetic peak exists. We also check target surface roughness effect on the final ion energy spectrum. Simulation results show when the roughness is controlled within 10% of the target thickness the final spectrum keeps monoenergetic character well, which is quite beneficial to the experiments. The detailed simulation results on the target parameter effect will be shown in our following paper.

In conclusion, by target shaping we have improved both the monochromaticity and collimation of the accelerated ions. The shaped target makes the ion acceleration much more uniform in the transverse direction as compared with the plain flat target and suppresses electron heating. Because of the absence of laser focusing by the natural cone, the maximum cutoff ion energy is smaller in the shaped target case. However, more ions are concentrated in the quasi-monoenergetic peak.

This work is supported by the DFG programs TR18 and GRK1203. M. C. acknowledges support by the Alexander von Humboldt Foundation. Z. M. S. is supported in part by the National Nature Science Foundation of China (Grants No. 10674175, No. 10734130) and the National Basic Research Program of China (Grant No. 2007CB815100).

- 
- [1] A. Pukhov, Phys. Rev. Lett. **86**, 3562 (2001); M. Hegelich *et al.*, *ibid.* **89**, 085002 (2002); T. Esirkepov *et al.*, *ibid.* **89**, 175003 (2002); T. Esirkepov *et al.*, *ibid.* **92**, 175003 (2004); J. Denavit, *ibid.* **69**, 3052 (1992); L. O. Silva *et al.*, *ibid.* **92**, 015002 (2004); J. Fuchs *et al.*, Nature Phys. **2**, 48 (2006); B. M. Hegelich *et al.*, Nature (London) **439**, 441 (2006); T. Ditmire *et al.*, *ibid.* **386**, 54 (1997); L. Yin *et al.*, Phys. Plasmas **14**, 056706 (2007); M. Chen *et al.*, *ibid.* **14**, 113106 (2007); J. H. Bin *et al.*, *ibid.* **16**, 043109 (2009).
  - [2] E. Fourkal *et al.*, Med. Phys. **34**, 577 (2007).
  - [3] M. Borghesi *et al.*, Phys. Plasmas **9**, 2214 (2002).
  - [4] N. Naumova *et al.*, Phys. Rev. Lett. **102**, 025002 (2009); M. Roth *et al.*, Phys. Rev. Lett. **86**, 436 (2001).
  - [5] A. P. L. Robinson *et al.*, New J. Phys. **10**, 013021 (2008); O. Klimo *et al.*, Phys. Rev. ST Accel. Beams **11**, 031301 (2008); X. Q. Yan *et al.*, Phys. Rev. Lett. **100**, 135003 (2008).
  - [6] X. Zhang *et al.*, Phys. Plasmas **14**, 123108 (2007).
  - [7] A. Macchi *et al.*, Phys. Rev. Lett. **94**, 165003 (2005).
  - [8] F. Pegoraro *et al.*, Phys. Rev. Lett. **99**, 065002 (2007).
  - [9] M. Chen *et al.*, Phys. Plasmas **15**, 113103 (2008).
  - [10] S. V. Bulanov *et al.*, Plasma Phys. Rep. **28**, 453 (2002); T. Okada *et al.*, Phys. Rev. E **74**, 026401 (2006); R. Sonobe *et al.*, Phys. Plasmas **12**, 073104 (2005); H. Schworer *et al.*, Nature (London) **439**, 445 (2006).
  - [11] A. Pukhov, J. Plasma Phys. **61**, 425 (1999).
  - [12] L. Cao *et al.*, Phys. Rev. E **78**, 036405 (2008).
  - [13] A. P. L. Robinson *et al.*, Plasma Phys. Controlled Fusion **51**, 024004 (2009).